Asia-Pac. J. Atmos. Sci., 53(2), 1-14, 2017
DOI:10.1007/s13143-017-0031-6
pISSN 1976-7633 / eISSN 1976-7951

Baseline Predictability of Daily East Asian Summer Monsoon Circulation Indices

Shucong Ai[1,2], Quanliang Chen[1], Jianping Li[3], Ruiqiang Ding[1,2], and Quanjia Zhong[2,4]

[1]*College of Atmospheric Science, Chengdu University of Information Technology, and Plateau Atmospheric and Environment Laboratory of Sichuan Province, Chengdu, China*
[2]*State Key Laboratory of Numerical Modeling for Atmospheric Sciences and Geophysical Fluid Dynamics (LASG), Institute of Atmospheric Physics, Chinese Academy of Sciences, Beijing, China*
[3]*College of Global Change and Earth System Sciences (GCESS), Beijing Normal University, Beijing, China*
[4]*College of Earth Science, University of Chinese Academy of Sciences, Beijing, China*

(Manuscript received 24 November 2016; accepted 13 April 2017)

Abstract: The nonlinear local Lyapunov exponent (NLLE) method is adopted to quantitatively determine the predictability limit of East Asian summer monsoon (EASM) intensity indices on a synoptic timescale. The predictability limit of EASM indices varies widely according to the definitions of indices. EASM indices defined by zonal shear have a limit of around 7 days, which is higher than the predictability limit of EASM indices defined by sea level pressure (SLP) difference and meridional wind shear (about 5 days). The initial error of EASM indices defined by SLP difference and meridional wind shear shows a faster growth than indices defined by zonal wind shear. Furthermore, the indices defined by zonal wind shear appear to fluctuate at lower frequencies, whereas the indices defined by SLP difference and meridional wind shear generally fluctuate at higher frequencies. This result may explain why the daily variability of the EASM indices defined by zonal wind shear tends be more predictable than those defined by SLP difference and meridional wind shear. Analysis of the temporal correlation coefficient (TCC) skill for EASM indices obtained from observations and from NCEP's Global Ensemble Forecasting System_(GEFS) historical weather forecast dataset shows that GEFS has a higher forecast skill for the EASM indices defined by zonal wind shear than for indices defined by SLP difference and meridional wind shear. The predictability limit estimated by the NLLE method is shorter than that in GEFS. In addition, the June-September average TCC skill for different daily EASM indices shows significant interannual variations from 1985 to 2015 in GEFS. However, the TCC for different types of EASM indices does not show coherent interannual fluctuations.

Key words: predictability at a synoptic timescale, East Asian summer monsoon, nonlinear local Lyapunov exponent

1. Introduction

The East Asian summer monsoon (EASM) is an important and unique component of the Asian summer monsoon system (e.g., Chen and Chang, 1980; Tao and Chen, 1987; Ding et al., 1992; Wang and Li, 2004). It is characterized by unique orographic forcing, involving huge thermal contrasts between the largest global continent, Eurasia, and the largest ocean basin, the Pacific. The EASM is also strongly influenced by the Tibetan Plateau, which is the highest land feature in the world. Floods and droughts associated with the EASM affect the livelihoods of billions of people and infrastructure across East Asia (EA) including China, Korea, and Japan (Huang et al., 2002, 2003). The variation of the EASM intensity is closely related to precipitation in EA (e.g., Li and Zeng, 2002; Huang et al., 2004). Thus, improving the prediction skill of the EASM intensity has great societal importance and economic value.

Many previous studies have examined the predictability and prediction skill of the monthly- or seasonal-scale circulation and rainfall of the EASM using numerical simulation. (e.g., Zeng, 1994; Sperber et al., 2001; Kang et al., 2002; Chang, 2004; Ding et al., 2004; Wang et al., 2004; Kang and Park, 2007; Wu and Li, 2008; Lee et al., 2010; Zhou and Zou, 2010; Ding et al., 2013). For example, Lee et al. (2010) used two climate forecast models (the NCEP Climate Forecast System and the Australia Meteorology Research Center Predictive Model) to investigate deficiencies and potential for predicting EASM precipitation and circulation one or two seasons ahead. Their results showed that both coupled models have difficulty in predicting summer mean precipitation anomalies, but are capable of predicting zonal wind anomalies at 850 hPa several months ahead. Wang and Lee (2004) found that almost all atmospheric general circulation models (AGCMs) have poor skill at simulating circulation and precipitation anomalies over the area from EA to the western North Pacific. Based on seven ensemble forecast models, Sperber et al. (2001) evaluated the seasonal predictability of rainfall and 850-hPa wind for the ASM, and reported that 850-hPa wind and rainfall from model hindcasts show limited prediction skill in EA. Wang et al. (2008a) found that the multi-model ensemble prediction skill for the EASM is better than the average skill of all individual models, which provides an effective way to predict EASM variability. In addition, previous studies investigated variability in the seasonal predictability of the EASM (e.g., Wang et al., 2005; Wu et al., 2009; Zhou and Zou, 2010; Yang et al., 2012; Seo et al., 2015), revealing that the El Niño-Southern Oscil-

Corresponding Author: Ruiqiang Ding, State Key Laboratory of Numerical Modeling for Atmospheric Sciences and Geophysical Fluid Dynamics (LASG), Institute of Atmospheric Physics, Chinese Academy of Sciences, Beijing 100029, China.
E-mail: drq@mail.iap.ac.cn

lation (ENSO) is the main source of seasonal predictability of the EASM.

These studies greatly improved our understanding of seasonal predictability of the EASM, and provide useful information about the prediction of rainfall and circulation connected with the EASM. However, compared with the seasonal predictability of the EASM, few investigations have examined the predictability and prediction skill of the EASM at synoptic timescales. Weather forecast models have been widely used to investigate forecast skill for weather systems (e.g., Jacobson, 2001; Bélair et al., 2003), but have not yet been used to assess forecast skill for the EASM at a synoptic timescale. The synoptic variability of the monsoon intensity is closely connected with the summer monsoon onset and rainfall in East Asian (Li and Duan, 2011). Currently, China National Climate Center (CNCC) has operationally released the daily EASM intensity index (available online at http://cmdp.ncc-cma.net/Monitoring/EastAsian/eamidx.2016.gif). Therefore, it is important to investigate the synoptic-scale predictability and prediction skill of the EASM. In this paper, we focus on the predictability of the EASM intensity at a synoptic timescale.

Previous studies have generally assessed the predictability of seasonal-scale EASM variability by using two common approaches: a diagnostic approach (Shi et al., 2008) and a prognostic approach (e.g., Wu et al., 2009; Wang et al., 2013). The former approach usually explores the signal-to-noise ratio of the EASM, which measures the relative contribution of the potentially predictable climate signal component and the unpredictable climate noise component of the EASM (Shi et al., 2008). However, the signal-to-noise ratio method only provides a qualitative measure of seasonal predictability and cannot quantitatively determine the predictability limit of the EASM. The latter approach is based on an empirical model. Wu et al. (2009) established an empirical model by combining the ENSO and spring North Atlantic Oscillation (NAO) to predict interannual variation of the EASM. Wang et al. (2013) established a similar model using the western Pacific Subtropical High (WPSH) to predict the interannual variability of the EASM. However, both the diagnostic and prognostic approaches are only suitable for estimating the potential predictability of climate variability: they cannot be used to assess the predictability of the EASM at a synoptic timescale.

A new method based on the nonlinear local Lyapunov exponent (NLLE), which is a nonlinear extension of the traditional Lyapunov exponent concept, was introduced to investigate atmospheric and oceanic predictability using observational data (e.g., Chen et al., 2006; Ding and Li, 2007; Ding et al., 2008; Li and Ding, 2011). The atmospheric and oceanic predictability limit can be quantitatively determined over various timescales by using the NLLE method (e.g., Ding et al., 2010, 2011, 2016; Li and Ding, 2013). Accordingly, the predictability of the EASM at a synoptic timescale can be estimated using the NLLE approach.

The remainder of this paper is organized as follows. Section 2 introduces the NLLE approach and Section 3 describes the data, weather forecast model, and the various EASM indices. Section 4 examines the predictability limit of the EASM at a synoptic timescale based on observation, and Section 5 assesses the forecast skill of daily EASM indices in the operational weather forecast model. Finally, a summary and discussion are provided in Section 6.

2. Nonlinear Local Lyapunov Exponent (NLLE)

For any dynamical system, the NLLE λ is defined as

$$\lambda[\boldsymbol{x}(t_0), \delta(t_0), \tau] = \frac{1}{\tau}\ln\frac{\|\delta(t_0+\tau)\|}{\|\delta(t_0)\|}, \quad (1)$$

where $x(t_0)$ denotes an initial state in phase space, $\delta(t_0)$ is the initial error, t_0 is the initial time, τ is the evolution time, and $\delta(t_0+\tau)$ is the evolution error. The NLLE is different from the traditional Lyapunov exponent, which is determined solely by the initial state $x(t_0)$ and the evolution time step τ, not by the initial error $\delta(t_0)$ (e.g., Yoden and Nomura 1993; Kazantsev 1999; Ziehmann et al., 2000). Moreover, the NLLE measures the average growth rate of initial errors based on the nonlinear error growth equations, thereby overcoming the limitations of the traditional Lyapunov exponent that uses the linearized error growth equation. The ensemble mean NLLE over the global attractor of the dynamical system is given by

$$\begin{aligned}\bar{\lambda}[\delta(t_0), \tau] &= \int_{\Omega} \lambda[\boldsymbol{x}(t_0), \delta(t_0), \tau]dx \\ &= \langle \lambda[\boldsymbol{x}(t_0), \delta(t_0), \tau]\rangle_N, \quad (N\to\infty)\end{aligned} \quad (2)$$

where Ω represents the domain of the global attractor of the system and $\langle\ \rangle_N$ denotes the ensemble average of samples of sufficiently large size N ($N\to\infty$). The ensemble mean NLLE reflects the global evolution of mean error growth over an attractor and can measure global mean predictability. The mean relative growth of the initial error (RGIE) can be obtained by:

$$\bar{\Phi}(\delta_0, \tau) = \exp[\bar{\lambda}(\delta_0, \tau)\tau]. \quad (3)$$

For chaotic systems, using the theorem from Ding and Li (2007), we obtain

$$\bar{\Phi}(\delta_0, \tau) \xrightarrow{P} c \quad (N\to\infty), \quad (4)$$

where $\xrightarrow{P}$ denotes the convergence in probability and c is a constant that depends on the converged probability distribution P of error growth.

For nonlinear dynamical systems, we can directly calculate the mean NLLE via a numerical integration of the error evolution equations. In addition, if large amounts of observational or experimental data are available from dynamic systems, we can estimate the mean NLLE by making use of these data when the evolution equations of systems are unknown or the known evolution equations are incomplete.

The general idea of the algorithm used to estimate mean

NLLE based on observational data is to find local dynamical analogs (LDAs) of the evolution pattern from an observational time series. The determination of LDAs is based on initial information and evolution information at two different time points in the time series. Considering that initial information in chaotic systems will gradually decay at an exponential rate, each step of evolution error within the evolution time interval is multiplied by a decreasing weighting coefficient at an exponential rate, which is estimated from the persistence of the observational time series. A brief description of the algorithm is given in Appendix A.

This NLLE method has been applied to atmospheric and oceanic observational data to investigate decadal changes in weather predictability (Ding et al., 2008), the temporal-spatial distributions of predictability limits of daily geopotential height and wind fields (Li and Ding, 2011), the temporal-spatial distributions of predictability limits of monthly and seasonal means of various climate variables (Li and Ding, 2013), the predictability limit of the intraseasonal oscillation (ISO) (Ding et al., 2010, 2011), the limit of decadal-scale climate predictability (Ding et al., 2016), and the application of nonlinear local Lyapunov vectors to ensemble predictions in Lorenz systems (Feng et al., 2014).

3. Data

a. Observations

Observation datasets employed in this study include daily wind and sea level pressure (SLP) fields from National Centers for Environmental Prediction-National Center for Atmospheric Research (NCEP/NCAR) reanalysis data for the period 1948-2015, gridded at $2.5^{o} \times 2.5^{o}$ resolution (Kalnay et al., 1996).

b. Description of the model and retrospective forecast

Daily wind and SLP fields from historical weather forecast datasets were generated with the 2012 version of NCEP's Global Ensemble Forecasting System. This reforecast version 2 dataset consists of an 11-member ensemble of forecasts, produced every day from 0000 UTC initial conditions from December 1984 to present (available online at www.esrl.noaa.gov/psd/forecasts/reforecast2/). The horizontal resolution of GEFS is T254 (about 50 km) out to 8 days, and T190 (about 70 km) from 8 to 16 days, and real-time forecasts are ongoing. For additional details on the GEFS, see Hamill et al. (2011a).

c. Monsoon indices

The EASM has complex spatial and temporal structures, and is influenced by variability originating in the tropics and mid-high latitudes (e.g., Chen and Chang, 1980; Huang and Lu, 1989; Wu et al., 2000; Enomoto et al., 2003; Ding, 2004; Ninomiya, 2004; He et al., 2006; Wu et al., 2006). The EASM has more complicated rainfall structures than the Indian summer monsoon, which results in difficulties in representing EASM strength using rainfall data. Consequently, large-scale winds are preferred for defining the broad-scale monsoon characteristics, meaning that most investigators define a simple EASM index using circulation parameters instead of rainfall. At least 25 circulation indices have been proposed to measure EASM intensity (Wang et al., 2008). Unfortunately, the representation of EASM circulation strength remains controversial. Therefore, considering that it is difficult to measure variability in EASM intensity with one index alone, six commonly used EASM indices belonging to three categories of monsoon circulation are employed in this study, as follows (Table 1).

Table 1. Description of three categories of EASM circulation indices. All indices are composed of two parts (Part I and Part II) and can thus be defined as follows: Index = Part I – Part II.

Index	Part I	Part II
I-SZ	SLP(20^{o}-50^{o}N, 110^{o}E)	SLP((20^{o}-50^{o}N, 160^{o}E)
I-ZZ	SLP(30^{o}-40^{o}N, 160^{o}E)	SLP(40^{o}-50^{o}N, 110^{o}E)
I-WF	U_{850}(5^{o}-15^{o}N, 90^{o}-130^{o}E)	U_{850}(22.5^{o}-32.5^{o}N, 110^{o}-140^{o}E)
I-ZTC	U_{850}(10^{o}-20^{o}N, 100^{o}-150^{o}E)	U_{850}(25^{o}-35^{o}N, 100^{o}-150^{o}E)
I-LKY	U_{200}(40^{o}-50^{o}N, 110^{o}-150^{o}E)	U_{200}(25^{o}-35^{o}N, 110^{o}-150^{o}E)
I-WYF	V_{850}(20^{o}-30^{o}N, 110^{o}-140^{o}E)	V_{850}(30^{o}-40^{o}N, 110^{o}-140^{o}E)

The first category uses the SLP gradient between land and sea to represent the east-west thermal contrast in EA. Shi and Zhu (1996; hereafter I-SZ) used the average SLP difference from 20^{o}N to 50^{o}N between 110^{o}E (Part I) and 160^{o}E (Part II) to represent monsoon strength. The index defined by Zhao and Zhou (2005; hereafter I-ZZ) is similar to the I-SZ, but the region is located at (30^{o}-40^{o}N, 160^{o}E) (Part I) and (40^{o}-50^{o}N, 110^{o}E) (Part II).

The second category is a zonal wind shear index that employs the north-south shear of zonal winds to express EASM variability. Wang and Fan (1999; hereafter I-WF) used the area-average 850-hPa zonal wind (U_{850}) over (5^{o}-15^{o}N, 90^{o}-130^{o}E) (Part I) minus the area-average U_{850} over (22.5^{o}-32.5^{o}N, 110^{o}-140^{o}E) (Part II) to define EASM intensity indices. Zhang et al. (2003; hereafter I-ZTC) applied a similar vorticity index, defined as the area-averaged zonal wind anomaly shear between (10^{o}-20^{o}N, 100^{o}-150^{o}E) (Part I) and (25^{o}-35^{o}N, 100^{o}-150^{o}E) (Part II) to measure monsoon strength. Lau et al. (2000; hereafter I-LKY) used the area-averaged 200-hPa zonal wind (U_{200}) difference between (40^{o}-50^{o}N, 110^{o}-150^{o}E) (Part I) and (25^{o}-35^{o}N, 110^{o}-150^{o}E) (Part II) to measure variations in the upper-tropospheric westerly jet stream associated with the EASM.

The third category is the meridional wind shear index that employs the north-south shear of meridional wind to measure variability in the EASM. For example, Wang et al. (2001; hereafter I-WYF) applied an area-average 850-hPa meridional wind (V_{850}) anomaly shear between (20^{o}-30^{o}N, 110^{o}-140^{o}E) (Part I) and (30^{o}-40^{o}N, 110^{o}-140^{o}E) (Part II) to measure the converging wind component of the EASM.

Daily monsoon intensity indices were used to measure variability in the EASM on a synoptic timescale. These indices are based on traditional definitions of EASM indices, but are calculated with daily rather than monthly data. The forecast skill of NCEP's GEFS historical weather forecast is measured by the temporal correlation coefficient (TCC) skill. The TCC skill was obtained from correlation coefficients between EASM indices calculated from the NCEP reanalysis dataset and from NCEP's GEFS historical weather forecast dataset. Higher correlation coefficients indicate a higher GEFS prediction skill.

4. Predictability of EASM indices at a synoptic timescale from observations

Using daily EASM indices for June-September (JJAS), the NLLE approach was applied to obtain the mean RGIE of six EASM indices (Fig. 1). The mean RGIE of all six EASM indices increases quickly initially, then slows and finally reaches saturation level. These processes represent linear fast growth, nonlinear slow growth, and saturation phases of the mean error in a chaotic system, respectively (Ding et al., 2008, 2016). In comparison, the mean RGIE of daily EASM indices defined by SLP difference (I-SZ and I-ZZ) and meridional wind shear (I-WYF) show faster growth than those from indices defined by zonal wind shear (I-WF, I-ZTC, and I-LKY).

The predictability limits of daily EASM indices can be quantitatively determined using the saturation value, given fact that most of information is lost from the initial state when the error growth reaches saturation (Ding and Li, 2008a, 2011). Figure 2 shows that daily EASM indices defined by zonal wind shear (I-WF, I-ZTC, and I-LKY) have a common predictability limit of around 7 days, which is higher than the limit of daily EASM indices defined by SLP difference (I-SZ and I-ZZ) and meridional wind shear (I-WYF) of about 5 days. This suggests that the daily variability of EASM indices represented

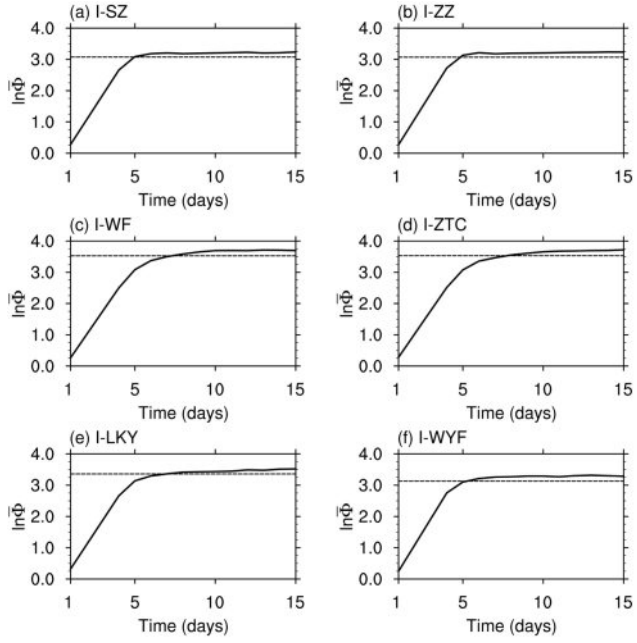

Fig. 1. Mean error growth for six daily EASM indices based on observation for the period 1948-2015: (a) I-SZ, (b) I-ZZ, (c) I-WF, (d) I-ZTC, (e) I-LKY, and (f) I-WYF, as obtained using the NLLE method. The dashed line represents the 95% level of the saturation value obtained by taking the average of the mean error growth after 10 days.

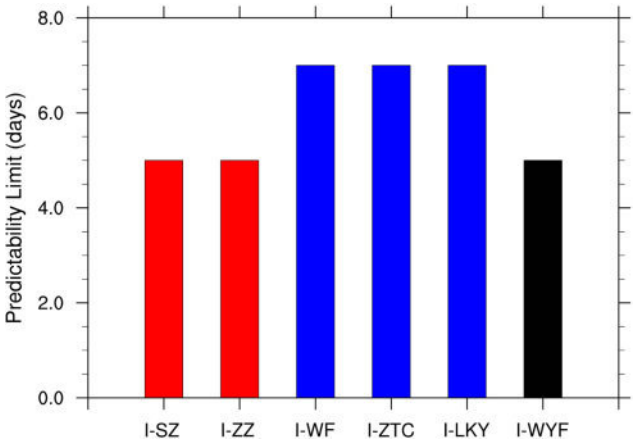

Fig. 2. Predictability limits of the six daily EASM indices based on observation for the period 1948-2015. The red bar indicates the predictability limit of the indices defined by SLP difference (I-SZ and I-ZZ), the blue bar represents the predictability limit of indices defined by zonal wind shear (I-WF, I-ZTC, and I-LKY), and the black bar denotes the predictability limit of indices defined by meridional wind shear (I-WYF).

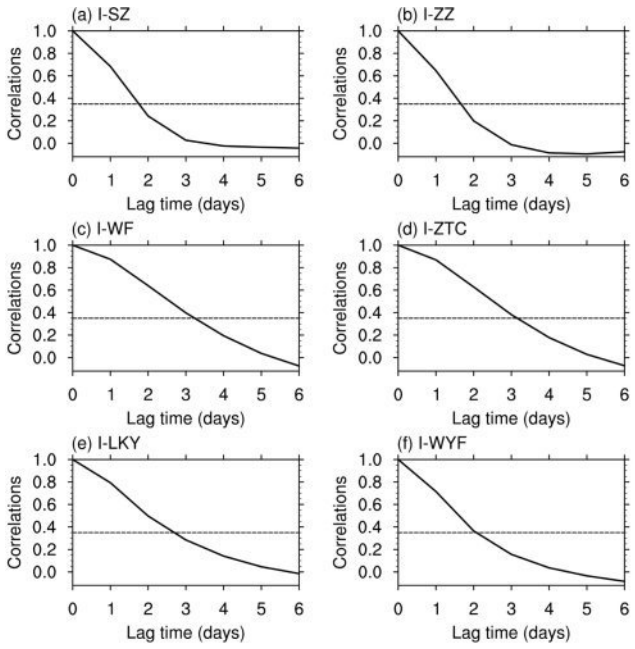

Fig. 3. Autocorrelations of the six daily EASM indices based on observation for the period 1948-2015: (a) I-SZ, (b) I-ZZ, (c) I-WF, (d) I-ZTC, (e) I-LKY, and (f) I-WYF. The horizontal dashed line denotes the 95% significance level.

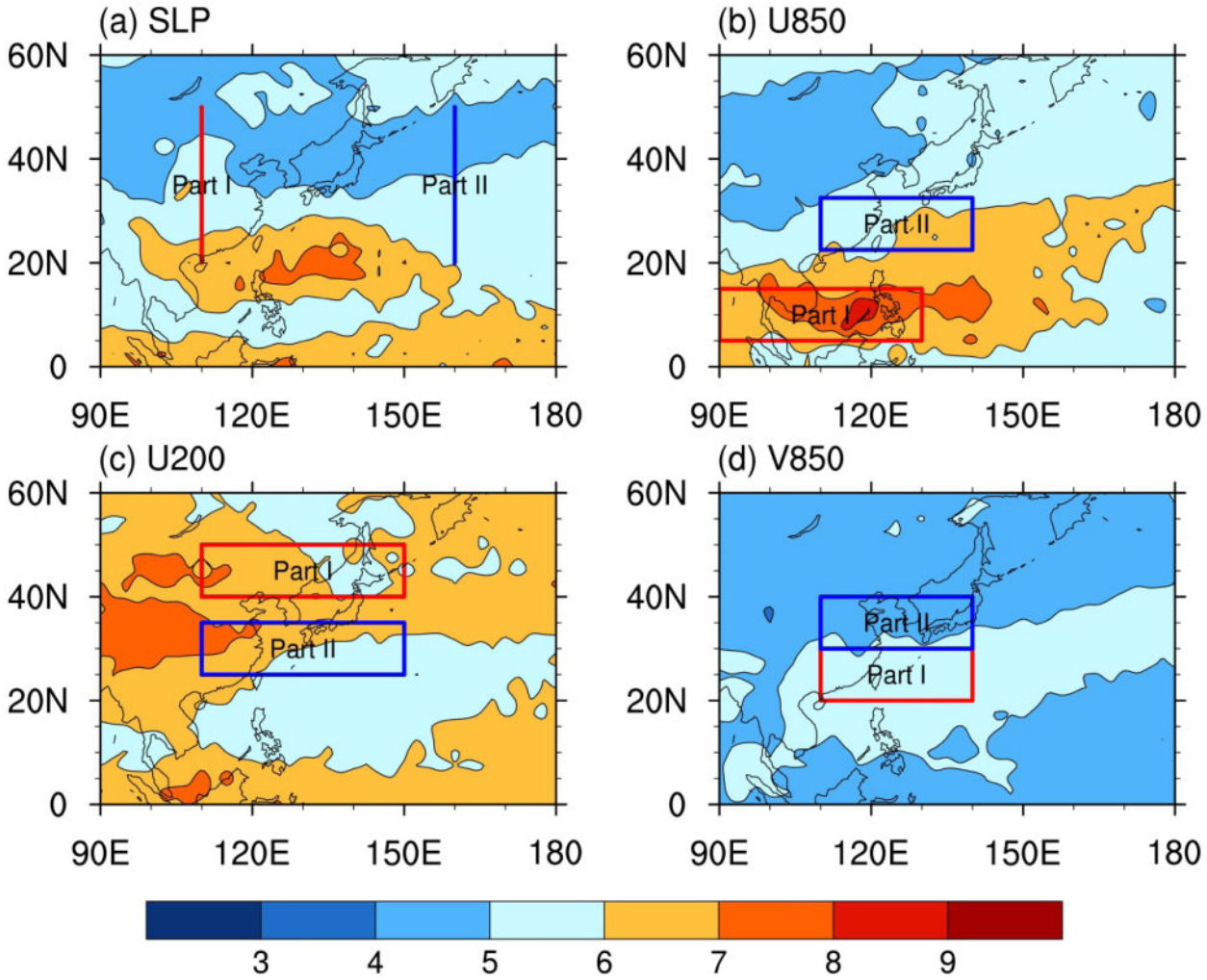

Fig. 4. Spatial distribution of the summer mean predictability limit (in days) in EA of: (a) daily SLP from I-SZ, (b) daily zonal wind at 850-hPa from I-WF, (c) daily zonal wind at 200-hPa from I-LKY, and (d) daily meridional wind shear at 850-hPa from I-WYF for the period 1948-2015. In all cases the red and blue boxes delineate Part I and II of each index, respectively.

by zonal wind shear (I-WF, I-ZTC, and I-LKY) may be more predictable than those represented by SLP difference (I-SZ and I-ZZ) and meridional wind shear (I-WYF). These results are generally consistent with the findings of Zhou and Zou (2010), who examined seasonal predictability of two commonly used EASM strength indices and revealed that the EASM index derived from zonal wind shear is more predictable than the index derived from SLP difference.

Atmospheric persistence represents the inherent long initial condition memory of the atmosphere (e.g., Reichler and Roads, 2004; Ding et al., 2008). Generally speaking, a long persistence is favorable for high predictability. Therefore, we further explore the daily persistence of various EASM indices with the aim of testing whether the predictability of various EASM indices is closely related to their persistence. The persistence of the EASM index is measured by the lag time (in days) for the autocorrelation of the daily EASM index to reach a significance level of 0.05 (e.g., Trenberth, 1985; Reichler and Roads, 2004). Daily EASM indices defined by SLP difference (I-SZ and I-ZZ) and meridional wind shear (I-WYF) exhibit relatively low persistence (about 2 days), while daily EASM indices defined by zonal wind shear (I-WF, I-ZTC, and I-LKY) exhibit relatively high persistence (about 3 days) (Fig. 3). These persistence results suggest that EASM indices defined by zonal wind shear (I-WF, I-ZTC, and I-LKY) tend to be more predictable than EASM indices defined by SLP difference (I-SZ and I-ZZ) and meridional wind shear (I-WYF). This finding is consistent with the predictability results shown above.

To understand the possible reasons why different EASM indices have varying predictability limits, we investigate the spatial distribution of the summer mean predictability limit of daily SLP, 850-hPa zonal wind, 200-hPa zonal wind, and 850-hPa meridional wind fields over EA (0°-60°N, 90°-180°E) (Fig. 4). The predictability limit of daily SLP shows a zonal distribution over EA, with a relatively high predictability limit

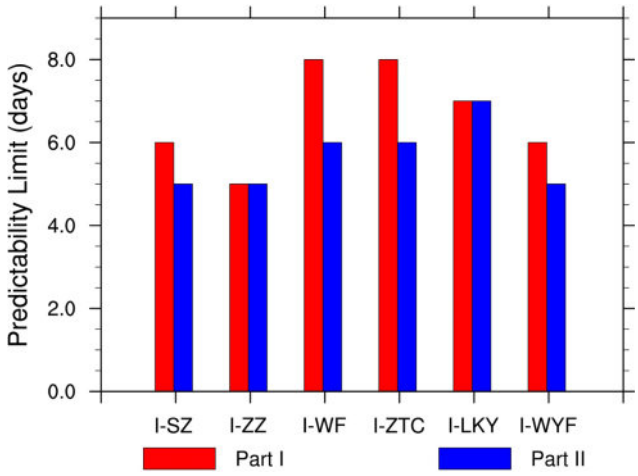

Fig. 5. Predictability limits of Part I and II of the six daily EASM indices based on observation for the period 1948-2015. The red bar indicates the limit of Part I, and the blue bar indicates the limit of Part II.

(about 6-8 days) over low-latitudes across EA (south of 30°N) and a relatively low predictability limit (about 4-6 days) over mid-high latitudes across EA (north of 30°N). The predictability limit of daily 850-hPa zonal wind also shows a zonal distribution over EA, with values decreasing from low-latitudes to mid-high latitudes across EA. The predictability limit of daily 200-hPa zonal wind is larger over most parts of Asian continent (about 6-8 days) compared with oceanic regions around EA (about 5-7 days). Compared with the previous three fields, the predictability limit of daily 850-hPa meridional wind is small (only 4-6 days) over most regions of EA, suggesting that the meridional wind field is the most unpredictable of all four fields over EA.

We note that the predictability limit of daily SLP over the area 20°-50°N, 110°E (Part I of the I-SZ) (about 4-7 days) is lower than that of 850-hPa zonal wind over the area 5°-15°N, 90°-130°E (Part I of the I-WF) (about 6-9 days) (Figs. 4a, b). Also, SLP over the area 20°-50°N, 160°E (Part II of the I-SZ) shows a lower predictability limit (about 4-6 days) than 850-hPa zonal wind over the area 22.5°-32.5°N, 110°-140°E (Part II of the I-WF) (about 5-7 days) (Figs. 4a, b).

The error growth of both Part I and II of the daily EASM index defined by SLP difference (I-SZ) is consistently faster than that for Part I and II of the index defined by zonal wind shear (I-WF) (not shown). As a result of the combined role of Part I and II in daily EASM indices, the predictability limit of the I-SZ is relatively low compared with the I-WF. In addition, the predictability limit of 850-hPa meridional wind is significantly lower than that of 850-hPa zonal wind over most regions of EA (Figs. 4b, d). The predictability limit of both parts of the EASM index defined by meridional wind shear (I-WYF) is lower than that for the index defined by zonal wind shear (I-WF) (Fig. 5). As a result, the index defined by zonal wind shear (I-WF) tends to be more predictable than the index

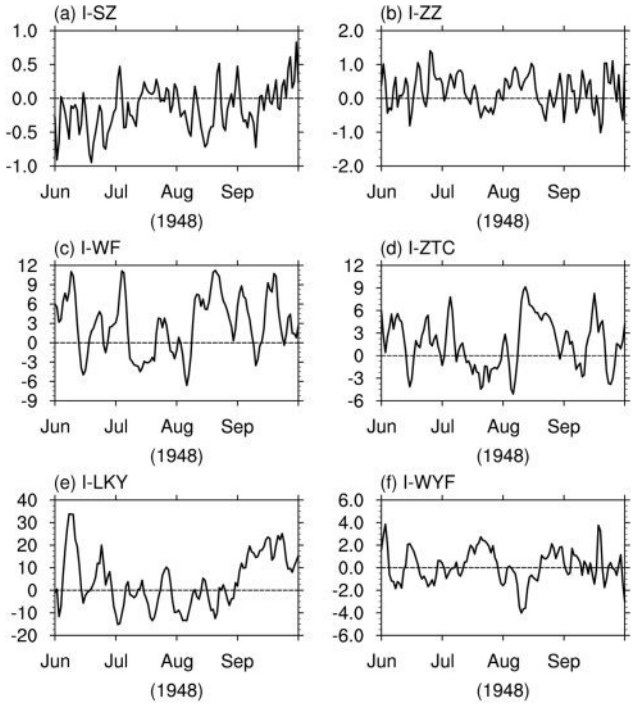

Fig. 6. Six different daily monsoon indices (solid line): (a) I-SZ, (b) I-ZZ, (c) I-WF, (d) I-ZTC, (e) I-LKY, and (f) I-WYF from 1 June 1948 to 30 September 1948. The annual cycle and linear trend of the indices have been removed.

defined by meridional wind shear (I-WYF).

We also examined the time series of the six EASM indices (Fig. 6). Note that EASM indices defined by SLP difference (I-SZ and I-ZZ) and meridional wind shear (I-WYF) exhibit more high-frequency daily fluctuations than indices defined by zonal wind shear (I-WF, I-ZTC, and I-LKY). The power spectra of different EASM indices reveal that variations in three monsoon indices defined by zonal wind shear (I-WF, I-ZTC, and I-LKY) appear to be concentrated at relatively long periods (> 10 days), whereas indices defined by SLP difference and meridional wind shear (I-SZ, I-ZZ, and I-WYF) occur mostly at higher frequencies, with periods of 5-8 days (Fig. 7). The high-frequency fluctuations of the I-SZ, I-ZZ, and I-WYF are expected to be more difficult to predict than low-frequency fluctuations of the I-WF, I-ZTC, and I-LKY. Shukla (1981) found that the lack of predictability is due mainly to the instabilities of synoptic-scale disturbances. High instability means low predictability. High-frequency fluctuation represents relative high instability, while low-frequency fluctuation represents relative low instability. This may explain why daily EASM indices defined by zonal wind shear (I-WF, I-ZTC, and I-LKY) have a higher predictability limit than indices defined by SLP difference (I-SZ and I-ZZ) and meridional wind shear (I-WYF). In addition, these results are generally consistent with the results of Ding et al. (2011), who examined the predictability limits of two commonly used winter MJO strength indices, and revealed that the low-frequency MJO

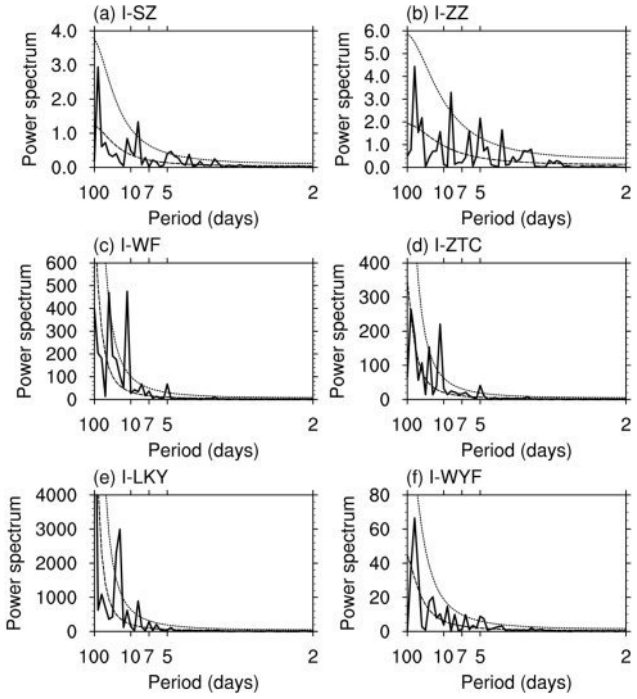

Fig. 7. Power spectral analysis of the daily vatiations of six daily EASM indices (solid line). The dotted line denotes 95% significance and the dashed line indicates the red noise line.

index (5 day moving average of daily index) is more predictable (25 days) than the high-frequency daily index (18 days).

5. Synoptic-scale forecast skill of EASM indices in weather forecast models'

The 31-year mean (1985-2015) TCC skill from six EASM indices in NCEP's GEFS historical weather forecast were used to assess whether different EASM indices have different forecast skills in weather forecast models (Fig. 8). The TCC skill of all six EASM indices decreases with forecast lead time. In comparison, the TCC skills of EASM indices defined by zonal wind shear (I-WF, I-ZTC, and I-LKY) are clearly higher than those defined by SLP difference (I-SZ and I-ZZ) and meridional wind shear (I-WYF). This suggests that the GEFS has a higher forecast skill for predicting indices defined by zonal wind shear than those defined by SLP difference and meridional wind shear.

Results based on observations for the period of 1985-2015 are consistent with results for the period of 1948-2015 (not shown). These findings in GEFS are consistent with results from observations presented above, and provide further evidence that EASM indices defined by zonal wind shear tend to be more predictable than indices defined by SLP difference and meridional wind shear. In addition, we note that EASM indices defined by SLP difference (I-SZ and I-ZZ) and meridional wind shear (I-WYF) have a similar predictability limit (about 5 days) in observations (Fig. 2). However, the forecast

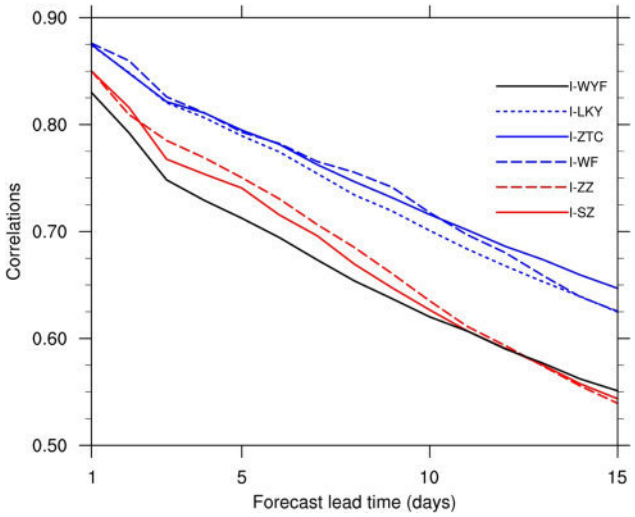

Fig. 8. TCC skills for six daily EASM indices averaged for 31 years from 1985-2015, obtained from the NCEP reanalysis dataset and the NCEP GEFS historical weather forecast dataset. The red, blue, and black lines represent the TCC skill of the indices defined by SLP difference (I-SZ and I-ZZ), zonal wind shear (I-WF, I-ZTC, and I-LKY), and meridional wind shear (I-WYF), respectively.

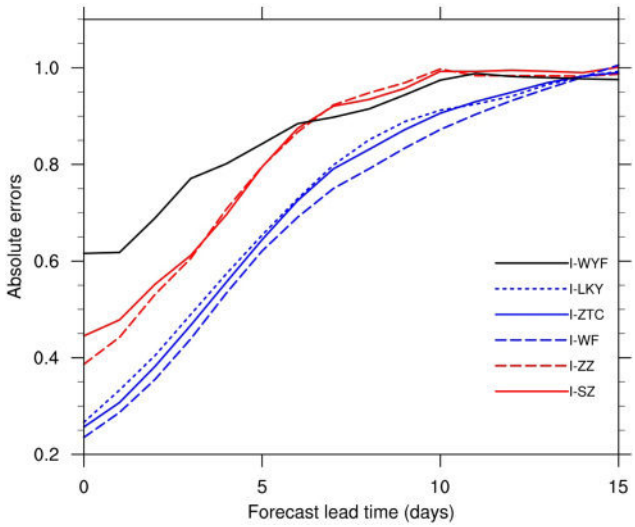

Fig. 9. Time evolution of the absolute errors of six daily EASM intensity indices obtained from the NCEP reanalysis dataset and the NCEP GEFS historical weather forecast dataset. The red, blue, and black lines represent the absolute errors of the indices defined by SLP difference (I-SZ and I-ZZ), zonal wind shear (I-WF, I-ZTC, and I-LKY), and meridional wind shear (I-WYF), respectively. Units of the indices have been removed.

skill of the I-WYF is lower than that of the I-SZ and I-ZZ in the GEFS, which is different from the results obtained from observations.

Figure 9 shows the time evolution of the absolute errors of six daily EASM indices in the GEFS, obtained from the difference between NCEP reanalysis and GEFS historical

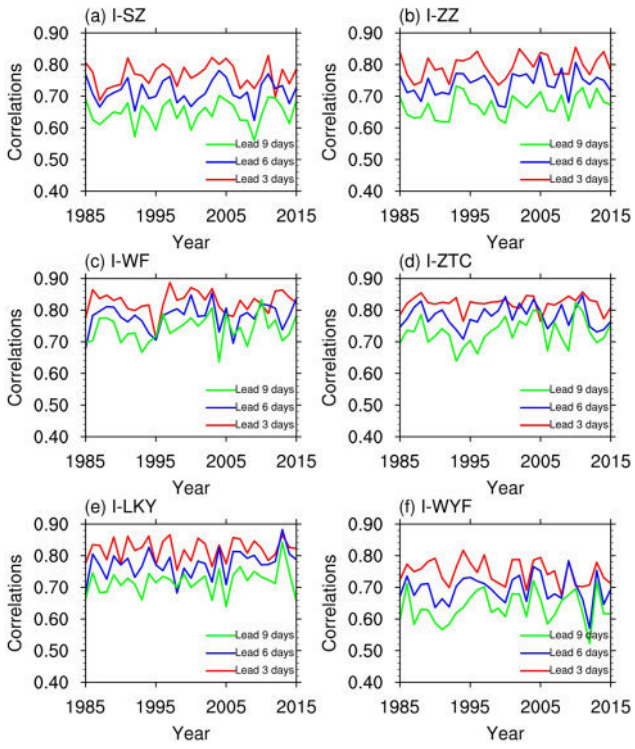

Fig. 10. TCC skills of six daily EASM indices for 31 years from 1985 to 2015 obtained from the NCEP reanalysis dataset and the NCEP GEFS historical weather forecast dataset. The red, blue, and green lines represent the TCC skill for forecast leads of 3, 6, and 9 days, respectively.

weather forecasts. The absolute errors of daily EASM indices defined by SLP difference (I-SZ and I-ZZ) and meridional wind shear (I-WYF) exhibit faster growth than those of indices define by zonal wind shear (I-WF, I-ZTC, and I-LKY). These results are consistent with conclusions derived from the data in Figs. 2 and 8, and further confirm the existence of differences between the predictabilities of various EASM indices. In addition, we note that the initial error of the daily EASM index defined by meridional wind shear (I-WYF) is high compared with that of other indices. This may explain why the forecast skill of the I-WYF is lowest among all six EASM indices in the GEFS.

In order to compare the predictability limit measured by NLLE with limit of forecast skill by GEFS, we estimate predictability limit of daily EASM indices in GEFS by using the 95% level of the saturation value of forecast error. The result shows that EASM indices defined by zonal wind shear have a predictability limit of around 10 days, which is higher than the predictability limit of EASM indices defined by SLP difference and meridional wind shear (about 8 days). This result is consistent with observational result. However, the predictability limit estimated by NLLE method is shorter than that in the GEFS.

We give some discussions of the possible reasons why the estimated predictability limit by the NLLE method is underestimated. First, the atmospheric and oceanic predictability depends not only on initial condition, but also on the slowly varying boundary conditions. However, the predictability of daily EASM indices obtained from the NLLE method mainly comes from the initial information, without including the predictability coming from slowly varying boundary condition. As a result, the estimated predictability of daily EASM indices by the NLLE method is shorter than the prediction skill by numerical models. Second, the NLLE method estimates the atmospheric and oceanic predictability by searching for the analogs from the observational time series. Nonetheless, it should be noted that if the number of observational points is not enough to find good analogs, the estimated predictability limit by the NLLE method would be underestimated.

Table 2. Correlation coefficients of TCC time series for six daily EASM indices with a 6-day forecast lead from 1985 to 2015. *Correlation is significant at the 95% level.

Correlation	I-SZ	I-ZZ	I-WF	I-ZTC	I-LKY	I-WYF
I-SZ	1	0.516*	–0.088	0.209	–0.013	0.034
I-ZZ		1	–0.089	–0.145	0.029	0.216
I-WF			1	0.464*	–0.288	–0.240
I-ZTC				1	–0.280	–0.024
I-LKY					1	0.26
I-WYF						1

Although the observational time series of daily EASM indices available cover periods of 68 years, it is likely to be not enough to find good analogues. Some false analogs are inevitably found in the observational time series of daily EASM indices, thereby leading to large initial errors that reduce the estimated predictability limit. This is one limitation of the NLLE method if we have only a relatively short period of observational data (Li and Ding, 2013).

Previous studies indicate that the seasonal predictability of the EASM shows significant interannual variation from the 1980s to 2000s (Yang et al., 2012). The JJAS-average TCC skill of different daily EASM indices also shows significant interannual variations from 1985 to 2015 in the GEFS (Fig. 10), which is similar to the seasonal predictability reported by Yang et al. (2012). For the same EASM index, the TCC skill shows largely consistent interannual fluctuations for different lead times. For example, for the I-SZ index, the correlation coefficients between the TCC skill for time series at lead times of 3 and 6 days and between the TCC skill for time series at lead times of 6 and 9 days are 0.65 and 0.85, respectively.

For a given lead time, the TCC skills of different types of EASM indices do not show coherent interannual fluctuations. For example, for a lead time of 6 days TCC skill for time series in the I-SZ and I-WF only have a correlation coefficient of −0.088 (Table 2). This suggests that the mechanisms responsible for interannual fluctuations of TCC skill for different types of daily EASM indices may be different.

It is generally accepted that the decadal changes of

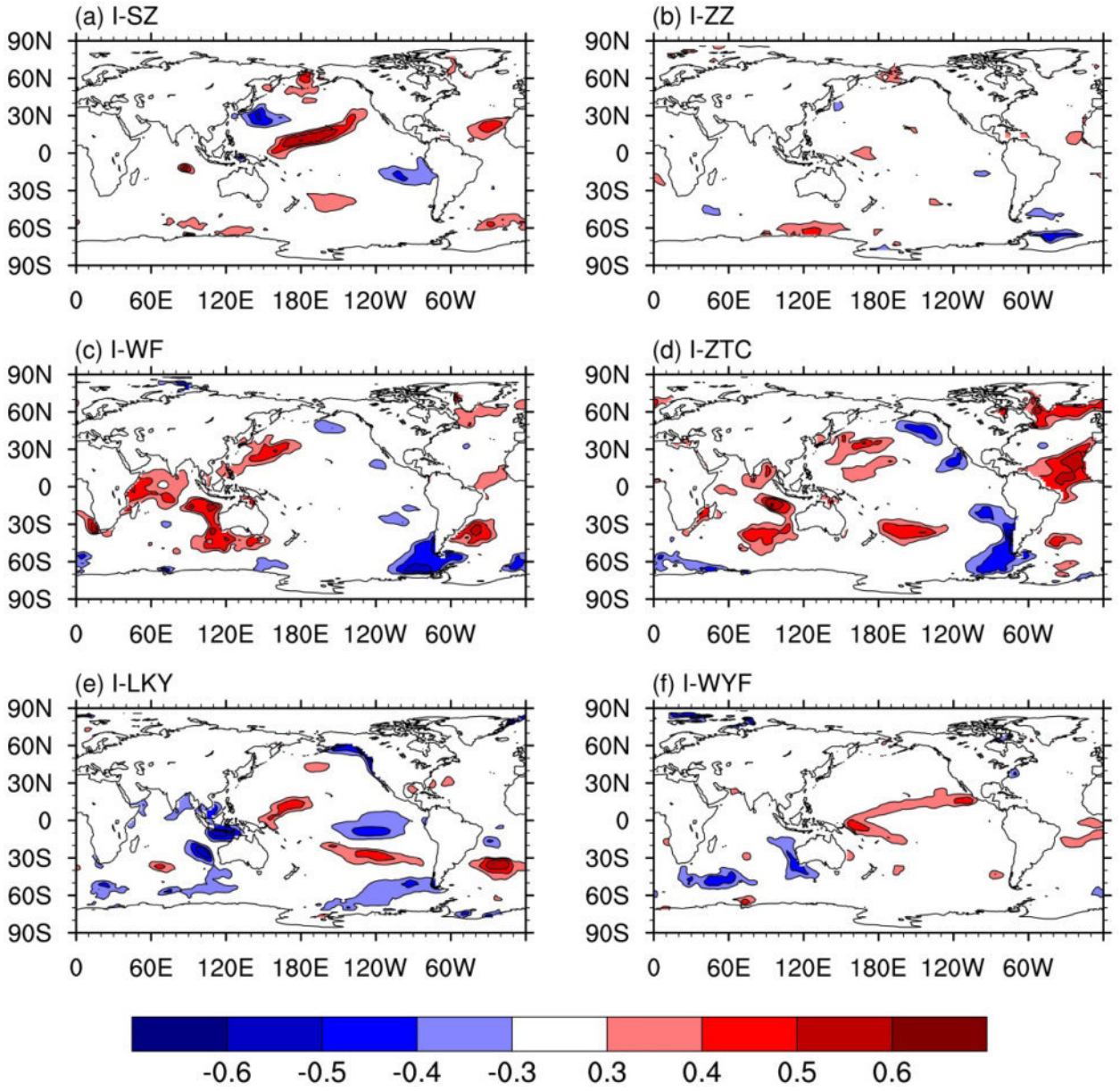

Fig. 11. Spatial distributions of correlations of the TCC time series with the previous winter (DJF) SST anomalies. In (a)-(f), shaded areas indicate correlations significant at the 90% level.

atmospheric predictability of monthly and seasonal means are generally associated with changes of external forcing, while the decadal changes of weather predictability are related to the changes of internal dynamics variability of the atmosphere (Ding et al., 2008). However, the changes of atmospheric general circulation and external forcing could modulate the dynamics of atmospheric internal variability, and in turn may change the atmospheric persistence and predictability. Therefore, we examine whether changes in the forecast skill of daily EASM indices are related to those of external forcing (such as SST). Figure 11 shows the correlations of TCC skill for time series of six daily EASM indices with the previous winter December-February (DJF) SST anomalies. There are significant SST signals in the North Pacific or tropical oceans for all six EASM indices. This suggests that changes in these SST signals may be related to interannual fluctuations of the forecast skill of daily EASM indices. However, the physical mechanisms responsible for the link between these SST signals and the forecast skill of daily EASM indices remain explained. Further research is necessary to examine the respective influences of these SST signals on the TCC skill of various EASM indices.

6. Summary and discussion

Based on the NLLE method, the predictability limit of daily

EASM indices at a synoptic timescale are quantitatively determined using the daily reanalysis dataset from NCEP. The results show that the predictability limits of EASM indices vary widely with the definition of the index. EASM indices defined by zonal wind shear have a limit of around 7 days, which is higher than the predictability limit of EASM indices defined by SLP difference and meridional wind shear (about 5 days). The initial errors of EASM indices defined by SLP difference and meridional wind shear show relatively rapid growth, while the initial errors of indices defined by zonal wind shear show relatively slow growth. The persistence of these results suggests that EASM indices defined by zonal wind shear tend to be more predictable than EASM indices defined by SLP difference and meridional wind shear. This finding is consistent with predictability results. Further analysis indicates that indices defined by zonal wind shear appear to fluctuate at relatively low frequencies, whereas indices defined by SLP difference and meridional wind shear occur mostly at higher frequencies. This result may explain why daily EASM indices defined by zonal wind shear have a higher predictability limit than indices defined by SLP difference and meridional wind shear.

By examining TCCs between EASM indices calculated from the NCEP reanalysis dataset and those from NCEP's GEFS historical weather forecast dataset, we found that the GEFS has a higher forecast skill in predicting EASM indices defined by zonal wind shear than indices defined by SLP difference and meridional wind shear. This finding is consistent with results from observations. Moreover, JJAS-average TCC skills for different daily EASM indices show significant interannual variations from 1985 to 2015 in the GEFS. However, the TCC skill of different types of EASM indices shows different interannual fluctuations.

The estimated predictability of daily EASM indices by the NLLE method is shorter than the prediction skill by numerical models. Although the predictability limit of daily EASM indices based on the NLLE method may be underestimated in the present study, the differences in the predictability limit of various EASM indices could be realistic. Results from numerical models indicate that daily EASM indices defined by zonal wind shear (I-WF, I-ZTC, and I-LKY) have a higher forecast skill than indices defined by SLP difference (I-SZ and I-ZZ) and meridional wind shear (I-WYF), which is consistent with observational results. In addition, the predictability of daily EASM indices measured by NLLE method can provide a baseline for the prediction skill of numerical models.

In this study, we used daily indices defined by circulation instead of precipitation due to the fact that unlike circulation variables (such as SLP or winds), the daily precipitation is not continuous. It is difficult to calculate the NLLE by using daily precipitation. Therefore, this study does not give the analysis of the predictability limit of indices defined by precipitation. However, the EASM index defined by air mass (Seo et al., 2015; hereafter I-SSLP), which is measured by meridional gradient of equivalent temperature, is a good supplement in this study. Figure 12 shows that daily EASM index defined by air mass has a predictability limit of about 7 days, which is close to the limit of the indices defined by zonal wind shear (I-WF, I-ZTC, and I-LKY) but higher than the limit of daily EASM indices defined by SLP difference (I-SZ and I-ZZ) and meridional wind shear (I-WYF) of about 5 days. Persistence, power spectral analysis and model forecasts of daily I-SSLP are also consistent with the results of indices defined by zonal wind shear (not shown).

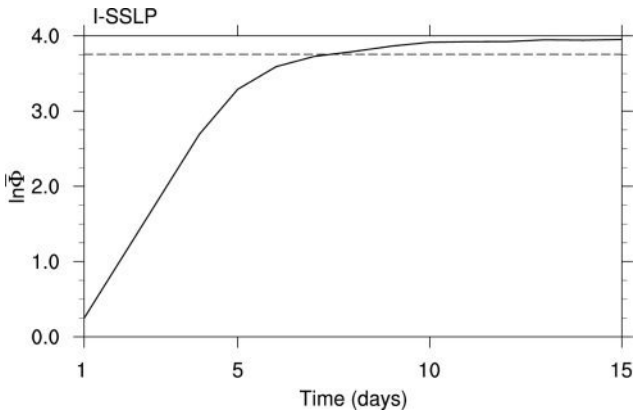

Fig. 12. Mean error growth for the daily EASM index based on observation for the period 1948-2015: I-SSLP, as obtained using the NLLE method. The dashed line represents the 95% level of the saturation value obtained by taking the average of the mean error growth after 10 days.

Variabilities of 5-day moving average of daily EASM circulation indices are closely linked to the onset and retreat of the EASM. Figure 13 shows that the 5-day moving average of various EASM indices has a similar predictability limit of about 13 days. This is different from the results of daily indices in which different types of EASM monsoon indices show different predictability. Persistence and power spectral analyses are also support the results of the predictability (not shown).

It should be noted that we only used NCEP/NCAR reanalysis datasets to calculate the predictability limits of EASM indices at a synoptic timescale. Previous studies have shown that the NCEP/NCAR reanalysis dataset has errors or uncertainties in some regions due to missing observations (eg., Kistler et al., 2001; Inoue and Matsumoto, 2004). Further work should compare the results of the predictability of the daily EASM indices obtained using NCEP reanalysis with those using other reanalysis or observational datasets. In addition, our results show that interannual variabilities in the TCC skill of daily EASM indices are complex. Different daily EASM indices, which reflect different variability in daily EASM strength, have different TCC skills. It is difficult to fully explain the interannual changes in the TCC skill of EASM indices at a synoptic timescale. Therefore, the mechanisms that determine the interannual variability in TCC skill for the EASM at a synoptic timescale require further study.

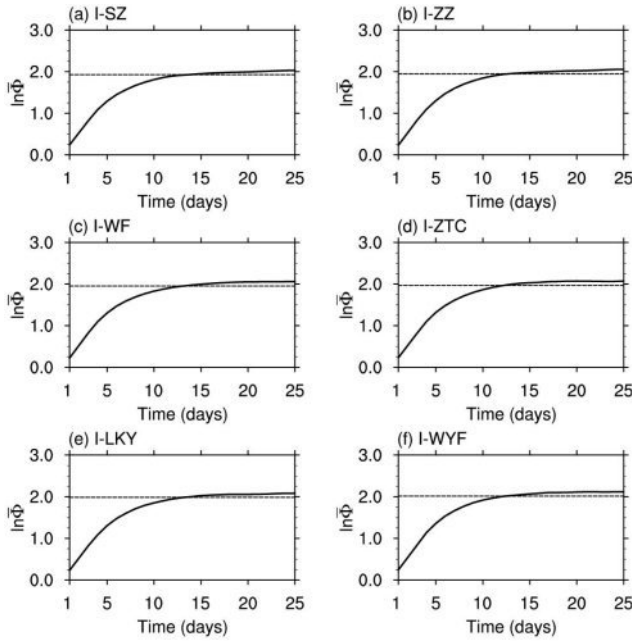

Fig. 13. Mean error growth for 5-day moving average of daily EASM circulation indices based on observation for the period 1948-2015: (a) I-SZ, (b) I-ZZ, (c) I-WF, (d) I-ZTC, (e) I-LKY, and (f) I-WYF, as obtained using the NLLE method. The dashed line represents the 95% level of the saturation value obtained by taking the average of the mean error growth after 10 days.

Acknowledgements. This work was funded by the National Key Technology Support Program (2015BAC03B07), the National Natural Science Foundation of China for Excellent Young Scholars (41522502), the 973 project of China (2016-YFA0601801), the China Special Fund for Meteorological Research in the Public Interest (GYHY201506013) and the Sichuan Youth Fund (2014JQ0019).

APPENDIX A

An algorithm for NLLE estimation from observational data

If we obtain the experimental data of a single variable x of an n-dimensional chaotic system, or observe the atmospheric or oceanic data of variable x at one point of n spatial grid points (e.g., the time series of x is given by $\{x(t_i),\ i = 0,1,2,\cdots\cdots,m-1\}$ where m represents the length of the time series), an algorithm that allows an estimation of the mean NLLE from the experimental or observational time series of variable x is as follows.

Step 1. Taking $x(t_0)$ as the reference point at time t_0, we first seek the local dynamical analog (LDA) $x(t_k)$ of the reference point from the raw series. Two distances (i.e., the initial distance between two points and the evolutionary distance between their trajectories within a short initial period) are used to measure the degree of similarity between the points. All points $x(t_j)$ ($|t_j - t_0| > t_D$, where t_D is the time taken for autocorrelations of variable x to drop to around 0.0, ensuring that a good analog pair is not merely due to persistence) in the raw series form a set S. The initial distance d_i between the points $x(t_0)$ and $x(t_j)$ is given by

$$d_i = |x(t_0) - x(t_j)|. \tag{A1}$$

We assume that the evolutions of the two points are analogous over a very short time τ, which is referred to as the initial evolutionary interval, if they are analogous at the initial time. The choice of the initial evolutionary interval τ depends on the persistence of variable x; if the persistence is low, the time over which two initially close points remain analogous is relatively short. The time taken for autocorrelations of variable x to drop to 0.9 can be regarded as a rough estimate of the initial evolutionary interval τ. A high value (0.9) of autocorrelation is chosen to ensure a short initial evolutionary interval (the results were found to be insensitive to the selected value). Within the initial evolutionary interval τ ($\tau = K\Delta$, where Δ is the sampling interval of the time series (i.e., $\Delta = t_i - t_{i-1}$) and K is the number of sampling intervals over the initial evolutionary interval), the evolutionary distance d_e between the two points $x(t_0)$ and $x(t_j)$ is given by:

$$d_e = \sqrt{\frac{1}{K+1}\sum_{i=0}^{K}[x(t_i) - x(t_{j+i})]^2}. \tag{A2}$$

Here, d_i is the amount of the initial separation between the two points $x(t_0)$ and $x(t_j)$, while d_e is the evolutionary distance between their trajectories over the initial evolutionary interval. The total distance d_t, considering not only the initial distance but also the evolutionary distance, is found by adding d_i and d_e:

$$d_t = d_i + d_e. \tag{A3}$$

If d_t is very small, it is highly likely that the points $x(t_0)$ and $x(t_j)$ are LDA points at the initial time. Of course, this approach is unlikely to exclude the possibility that only the variable x and its most relevant variables remain close, whereas other variables evolve very differently over time, especially for high-dimensional dynamical systems. Therefore, the analogs based on variable x are only local analogs, and they cannot simply be considered as global analogs. The constraint of the total distance d_t, which contains both initial information and evolutionary information over an initial evolutionary, allows us to exclude a large portion of all points with large initial distances, thereby helping us to find a truly local analog for the reference point.

For every point $x(t_j)$ in the set S, the value of d_t can be determined. The nearest neighbor (LDA) $x(t_k)$ of the reference point $x(t_0)$ can be chosen from the set S only if d_t is the minimum. Then, the initial distance between $x(t_0)$ and $x(t_k)$ is denoted as follows:

$$L_1(t_0) = |x(t_0) - x(t_k)|. \tag{A4}$$

Step 2. At time $\tau_i = i \times \Delta$ (i = 1, 2, 3, ……, M, where M is the total number of evolutionary steps), $x(t_0)$ will have evolved to $x(t_0 + \tau_i)$ along the reference trajectory, and $x(t_k)$ will have evolved into $x(t_k + \tau_i)$ along the analogous trajectory. The initial difference $L_1(\tau_0)$ will have become:

$$L_1(\tau_i) = \left| x(t_0 + \tau_i) - x(t_k + \tau_i) \right| . \quad \text{(A5)}$$

The growth rate of the initial error during the evolutionary interval (τ_i) is:

$$\xi_1(\tau_i) = \frac{1}{\tau_i} \ln \frac{L_1(\tau_i)}{L_1(0)}, \quad (i = 1, 2, 3, \cdots\cdots, M). \quad \text{(A6)}$$

With i gradually increasing, we can obtain the variation of $\xi_1(\tau_i)$ as a function of the evolution time τ_i (i = 1, 2, 3, ……, M).

Step 3. Taking $x(t_1)$ as the reference state and evolution time $\tau_i = i \times \Delta$ (i = 1, 2, 3, ……, M), and repeating Steps 1 and 2 above, we obtain the error growth rate $\xi_2(\tau_i)$ as a function of the evolution time τ_i :

$$\xi_2(\tau_i) = \frac{1}{\tau_i} \ln \frac{L_2(\tau_i)}{L_2(0)},$$

where $L_2(0)$ is the initial distance between the reference point $x(t_1)$ and its LDA, and $L_2(\tau_i)$ is the evolution of $L_2(0)$ with time τ_i.

Step 4. The above procedure is repeated until the trajectory reaches the last reference point $x(t_{m-M-1})$, and we have error growth rates at all reference points $\{x(t_0), x(t_1), \cdots\cdots, x(t_{m-M-1})\}$ given by:

$$\xi_k(\tau_i) = \frac{1}{\tau_i} \ln \frac{L_k(\tau_i)}{L_k(0)}, (k = 1, \cdots\cdots, N);\ i = 1, 2, 3, \cdots\cdots, M)$$

where $N = m - M$ is the total number of reference points on the reference trajectory, $\tau_i = i \times \Delta$ (i = 1, 2, 3, ……, M) is the evolution time, $L_k(0)$ is the initial distance between the reference point $x(t_k)$ and its LDA, and $L_k(\tau_i)$ is the evolution of $L_k(0)$ with the time τ_i. It follows that the average of error growth rates at all reference points is:

$$\bar{\xi}(\tau_i) = \frac{1}{N} \sum_{k=1}^{N} \xi_k(\tau_i)$$

$$= \frac{1}{N} \sum_{k=1}^{N} \left[\frac{1}{\tau_i} \ln \frac{L_k(\tau_i)}{L_k(0)} \right] = \frac{1}{\tau_i} \ln \left[\sqrt[N]{\frac{L_1(\tau_i)}{L_1(0)} \frac{L_2(\tau_i)}{L_2(0)} \cdots\cdots \frac{L_N(\tau_i)}{L_N(0)}} \right].$$

That is:

$$\exp[\bar{\xi}(\tau_i)\, \tau_i] = \sqrt[N]{\frac{L_1(\tau_i)}{L_1(0)} \frac{L_2(\tau_i)}{L_2(0)} \cdots\cdots \frac{L_N(\tau_i)}{L_N(0)}}. \quad \text{(A7)}$$

Step 5. Observing that the right-hand-side of Eq. (A7) is the geometric mean of the relative growth of initial error (RGIE) of all reference points, we obtained the approximation of the mean RGIE:

$$\bar{\Phi}(\tau_i) = \exp[\bar{\xi}(\tau_i)\, \tau_i], (i = 1, 2, 3, \cdots\cdots, M). \quad \text{(A8)}$$

By investigating the evolution of $\bar{\Phi}(t_i)$ with increasing τ_i, we can estimate the mean predictability limit of the variable x.

References

Bélair, S., L. P. Crevier, J. Mailhot, B. Bilodeau, and Y. Delage, 2003: Operational implementation of the ISBA land surface scheme in the Canadian regional weather forecast model. Part I: Warm season results. *J. Hydrometeor.*, **4**, 352-370, doi:10.1175/1525-7541(2003)4<352:OIOTIL>2.0.CO;2.

Chang, C. P., 2004: Preface. *East Asian Monsoon*. Chang, C.-P. Ed., World Scientific, v -vi.

Chen, B. H., J. P. Li, and R. Q. Ding, 2006: Nonlinear local Lyapunov exponent and atmospheric predictability research. *Sci. China Ser. D,* **49**, 1111-1120.

Chen, T. J. G., and C. P. Chang, 1980: The structure and vorticity budget of an early summer monsoon trough (Mei-Yu) over southeastern China and Japan. *Mon. Wea. Rev.,* **108**, 942-953.

Ding, R. Q., and J. P. Li, 2007: Nonlinear finite-time Lyapunov exponent and predictability. *Phys. Lett. A,* **364**, 396-400, doi:10.1016/j.physleta.2006.11.094.

_____, _____, and K.-J. Ha, 2008: Trends and interdecadal changes of weather predictability during 1950s-1990s. *J. Geophys. Res.,* **113**, D24112, doi:10.1029/2008JD010404.

_____, _____, and _____, 2008a: Nonlinear local Lyapunov exponent and quantification of local predictability. *Chinese Phys. Lett.,* **25**, 1919-1922.

_____, _____, and K. H. Seo, 2010: Predictability of the Madden-Julian oscillation estimated using observational data. *Mon. Wea. Rev.,* **138**, 1004-1013, doi:10.1175/2009MWR3082.1.

_____, _____, and _____, 2011: Estimate of the predictability of boreal summer and winter intraseasonal oscillations from observations. *Mon. Wea. Rev.,* **139**, 2421-2438, doi:10.1175/2011MWR3571.1.

_____, _____, F. Zheng, J. Feng, and D. Liu, 2016: Estimating the limit of decadal-scale climate predictability using observational data. *Climate Dyn.,* **46**, 1563-1580, doi:10.1007/s00382-015-2662-6.

Ding, Y. H., 1992: Summer monsoon rainfalls in China. *J. Meteor. Soc. Japan,* **70**, 397-421.

_____, 2004: Seasonal march of the east Asian summer monsoon. *East Asian Monsoon*. Chang, C.-P. Ed., World Scientific, 3-53.

_____, Y. Sun, and Y. Y. Liu, 2013: Interdecadal and interannual variabilities of the Asian summer monsoon and its projection of future change. *Chinese J. Atmos. Sci.,* **37**, 253-280 (in Chinese with English abstract).

Enomoto, T., B. J. Hoskins, and Y. Matsuda, 2003: The formation mechanism of the Bonin high in August. *Quart. J. Roy. Meteor. Soc.,* **129**, 157-178, doi:10.1256/qj.01.211.

Feng, J., R. Ding, D. Liu, and J. Li, 2014: The application of nonlinear local Lyapunov vectors to ensemble predictions in Lorenz systems. *J. Atmos. Sci.,* **71**, 3554-3567, doi:10.1175/JAS-D-13-0270.1.

Hamill, T. M., J. S. Whitaker, M. Fiorino, and S. G. Benjamin, 2011a: Global ensemble predictions of 2009's tropical cyclones initialized with an ensemble Kalman filter. *Mon. Wea. Rev.,* **139**, 668-688, doi:10.1175/2010MWR3456.1.

He, J. H., Z. W. Wu, Z. H. Jiang, C. S. Miao, and G. R. Han, 2006: "Climate effect" of the northeast cold vortex and its influences on Meiyu. *Chinese Sci. Bull.,* **51**, 2803-2809, doi:10.1007/s11434-007-0053-z (in Chinese with English abstract).

Huang, R. H., and L. Lu, 1989: Numerical simulation of the relationship between the anomaly of subtropical high over east Asia and the convective activities in the western tropical Pacific. *Adv. Atmos. Sci.,* **6**, 202-214 (in Chinese with English abstract).

_____, and L. T Zhou, 2002: Research on the characteristics, formation mechanism and prediction of severe climatic disasters in China. *J. Nat. Dis.,* **11**, 1-9 (in Chinese with English abstract).

_____, J. L. Chen, L. T. Zhou, and Q. Y. Zhang, 2003: Studies on the relationship between the severe climatic disasters in China and the East Asia climate system. *Chinese J. Atmos. Sci.,* **27**, 770-787 (in Chinese with English abstract).

_____, Q. Y. Zhang, and S. G. Ruan, 2004: *Prediction and Warning of Meteorological Disasters in China and Scientific Decision for the Prevent ion and Mitigation of These Disasters*. China Meteorological Press, 148 pp (in Chinese).

Inoue, T., and J. Matsumoto, 2004: A comparison of summer sea level pressure over east Eurasia between NCEP-NCAR reanalysis and ERA-40 for the period 1960-99. *J. Meteor. Soc. Japan,* **82**, 951-958.

Jacobson, M. Z., 2001: GATOR-GCMM: A global-through urban-scale air pollution and weather forecast model: 1. Model design and treatment of subgrid soil, vegetation, roads, rooftops, water, sea ice, and snow. *J. Geophys. Res.,* **106**, 5385-5401, doi:10.1029/2000JD900560.

Kalnay, E., and Coauthors, 1996: The NCEP/NCAR 40-year reanalysis project. *Bull. Amer. Meteor. Soc.,* **77**, 437-471.

Kang, H., and C. K. Park, 2007: Error analysis of dynamical seasonal predictions of summer precipitation over the East Asian-western Pacific region. *Geophys. Res. Lett.,* **34**, doi:10.1029/2007GL029392.

Kang, I. S., and Coauthors, 2002: Intercomparison of the climatological variations of Asian summer monsoon precipitation simulated by 10 GCMs. *Climate Dyn.,* **19**, 383-395, doi:10.1007/s00382-002-0245-9.

Kazantsev, E., 1999: Local Lyapunov exponents of the quasi-geostrophic ocean dynamics. *Appl. Math. Comput.,* **104**, 217-257, doi:10.1016/S0096-3003(98)10078-4.

Kistler, R. E., and Coauthors, 2001: The NCEP/NCAR 50-year reanalysis: Monthly means CD-ROM and documentation. *Bull. Amer. Meteor. Soc.,* **82**, 247-267.

Lau, K. M., K.-M. Kim, and S. Yang, 2000: Dynamical and boundary forcing characteristics of regional components of the Asian summer monsoon. *J. Climate,* **13**, 2461-2482.

Lee, S. S., J. Y. Lee, K. J. Ha, B. Wang, and J. K. E. Schemm, 2010: Deficiencies and possibilities for long-lead coupled climate prediction of the Western North Pacific-East Asian summer monsoon. *Climate Dyn.,* **36**, 1173-1188, doi:10.1007/s00382-010-0832-0.

Li, F., and A. M. Duan, 2011: Variation of the Tibetan Plateau summer monsoon and its effect on the rainfall and the circulation in Asia-A case study in 2008. *Chinese J. Atmos. Sci.,* **35**, 694-706 (in Chinese with English abstract).

Li, J. P., and R. Q. Ding, 2011: Temporal-spatial distribution of atmospheric predictability limit by local dynamical analogues. *Mon. Wea. Rev.,* **139**, 3265-3283, doi:10.1175/MWR-D-10-05020.1.

_____, and _____, 2013: Temporal-spatial distribution of the predictability limit of monthly sea surface temperature in the global oceans. *Int. J. Climatol.,* **33**, 1936-1947, doi:10.1002/joc.3562.

_____, and Q. Zeng, 2002: A unified monsoon index. *Geophys. Res. Lett.,* **29**, 1274, doi:10.1029/2001GL013874.

Ninomiya, K., 2004: Large-and mesoscale features of the Meiyu-baiu front associated with intense rainfalls. *East Asian Monsoon*. Chang, C.-P. Ed., World Scientific, 404-435.

Reichler, T., and J. O. Roads, 2004: Time-space distribution of long-range atmospheric predictability. *J. Atmos. Sci.,* **42**, 249-263.

Seo, K. H., J. H. Son, J. Y. Lee, and H. S. Park, 2015: Northern East Asian Monsoon precipitation revealed by air mass variability and its prediction. *J. Climate.,* **28**, 6221-6233, doi:10.1175/JCLI-D-14-00526.1.

Shi, H. B., T. J. Zhou, H. WAN, and B. Wang, 2008: SMIP2 Experiment-based qnalysis on the simulation and potential predictability of Asian summer monsoon. *Chinese J. Atmos. Sci.,* doi:10.3878/j.issn.1006-9895.2008.01.04 (in Chinese with English abstract).

Shi, N., and Q. G. Zhu, 1996: An abrupt change in the intensity of the East Asian summer monsoon index and its relationship with temperature and precipitation over East China. *Int. J. Climatol.,* **16**, 757-764 (in Chinese with English abstract).

Shukla, J., 1981: Dynamical predictability of Monthly means. *J. Atmos. Sci.,* **38**, 2547-2572.

Sperber, K. R., and Coauthors, 2001: Dynamical seasonal predictability of the Asian summer monsoon. *Mon. Wea. Rev.,* **129**, 2226-2248.

Tao, S. Y., and L. X. Chen, 1987: A review of recent research on the East Asian summer monsoon in China. *Monsoon Meteorology.* Chang, C. P. et al. Eds., Oxford University Press, 60-92.

Trenberth, K. E., 1985: Persistence of daily geopotential heights over the Southern Hemisphere. *Mon. Wea. Rev.,* **113**, 38-53.

Wang, B., and Z. Fan, 1999: Choice of South Asian summer monsoon indices. *Bull. Amer. Meteor. Soc.,* **80**, 629-638.

_____, and T. Li, 2004: East Asian monsoon and ENSO interaction. *East Asian Monsoon*. Chang, C. P. Ed., World Scientific, 172-212.

_____, I. S. Kang, and J. Y. Lee, 2004: Ensemble simulations of Asian-Australian monsoon variability by 11 AGCMs. *J. Climate,* **17**, 803-818.

_____, Q. Ding, X. Fu, I. S. Kang, K. Jin, J. Shukla, and F. Doblas-Reyes, 2005: Fundamental challenge in simulation and prediction of summer monsoon rainfall. *Geophys. Res. Lett.,* **32**, L15711, doi:10. 1029/2005GL022734.

_____, Z. Wu, J. Li, J. Liu, C. P. Chang, Y. Ding, and G. Wu, 2008: How to measure the strength of the East Asian summer monsoon. *J. Climate,* **21**, 4449-4463.

_____, and Coauthors, 2008a: Advance and prospectus of seasonal prediction: Assessment of the APCC/CliPAS 14-model ensemble retrospective seasonal prediction (1980-2004). *Climate Dyn.,* **33**, 93-117, doi:10.1007/s00382-008-0460-0.

_____, B. Q. Xiang, and J. Y. Lee, 2013: Subtropical high predictability establishes a promising way for monsoon and tropical storm predictions. *Proc. Natl. Acad. Sci.,* **110**, 2718-2722, doi:10.1073/pnas.1214626110.

Wang, Y. F., B. Wang, and J. H. Oh, 2001: Impacts of the preceding El Niño on the East Asian summer atmospheric circulation. *J. Meteor. Soc. Japan,* **79**, 575-588, doi:10.2151/jmsj.79.575.

Wu, G. X., P. Liu, Y. Liu, and W. Li, 2000: Impacts of sea surface temperature anomaly in the Indian Ocean on the subtropical cyclone over the western Pacific—Two-stage thermal adaptation in the atmosphere. *Acta Meteor. Sin*., **58**, 513-522 (in Chinese with English abstract).

Wu, Z. W., Z. H. Jiang, and J. H. He, 2006: Comparison analysis of flood and drought features among the first flood period in south China, Meiyu period in the Yangtze River and Huaihe River valleys and rainy season in north China in the last 50 years. *Chinese J. Atmos. Sci.,* **30**, 391-401 (in Chinese with English abstract).

_____, B. Wang, J. Li, and F. F. Jin, 2009: An empirical seasonal prediction model of the East Asian summer monsoon using ENSO and NAO. *J. Geophys. Res.,***114**, doi:10.1029/2009JD011733.

_____, and J. P Li, 2008: Prediction of the Asian-Australian monsoon interannual variations with the grid-point atmospheric model of IAP LASG (GAMIL). *Adv. Atmos. Sci.,* **25**, 387-394, doi:10.1007/s00376-008-0387-8.

Yang, D. J., Y. M. Tang, Y. C. Zhang, and X. Q. Yang, 2012: Information-based potential predictability of the Asian summer monsoon in a coupled model. *J. Geophys. Res.,* 117, doi:10.1029/2011JD016775.

Yoden, S., and M. Nomura, 1993: Finite-time Lyapunov stability analysis and its application to atmospheric predictability. *J. Atmos. Sci.,* **50**, 1531-1543.

Zeng, Q. C., 1994: Experiments of seasonal and extreseasonal predictions of summer monsoon precipitation. *Proc. International Conference on Monsoon Variability and Predicability.* Trieste, May 9-13, 1994, 452-459.

Zhang, Q. Y., S. Y. Tao, and L. T. Chen, 2003: The interannual variability of East Asian summer monsoon indices and its association with the pattern of general circulation over East Asia. *Acta Meteor. Sin*., **61**, 559-568 (in Chinese with English abstract).

Zhao, P., and Z. J. Zhou, 2005: East Asian subtropical summer monsoon index and its relationships to rainfall. *Acta Meteor. Sin*., **63**, 933-941 (in Chinese with English abstract).

Zhou, T. J., and L. W. Zou, 2010: Understanding the predictability of East Asian summer monsoon from the reproduction of land-sea thermal contrast change in AMIP-type simulation. *J. Climate,* **23**, 6009-6026, doi:10.1175/2010JCLI3546.1.

Ziehmann, C., L. A. Smith, and J. Kurths, 2000: Localized Lyapunov exponents and the prediction of predictability. *Phys. Lett. A,* **4**, 237-251, doi:10.1016/S0375-9601(00)00336-4.